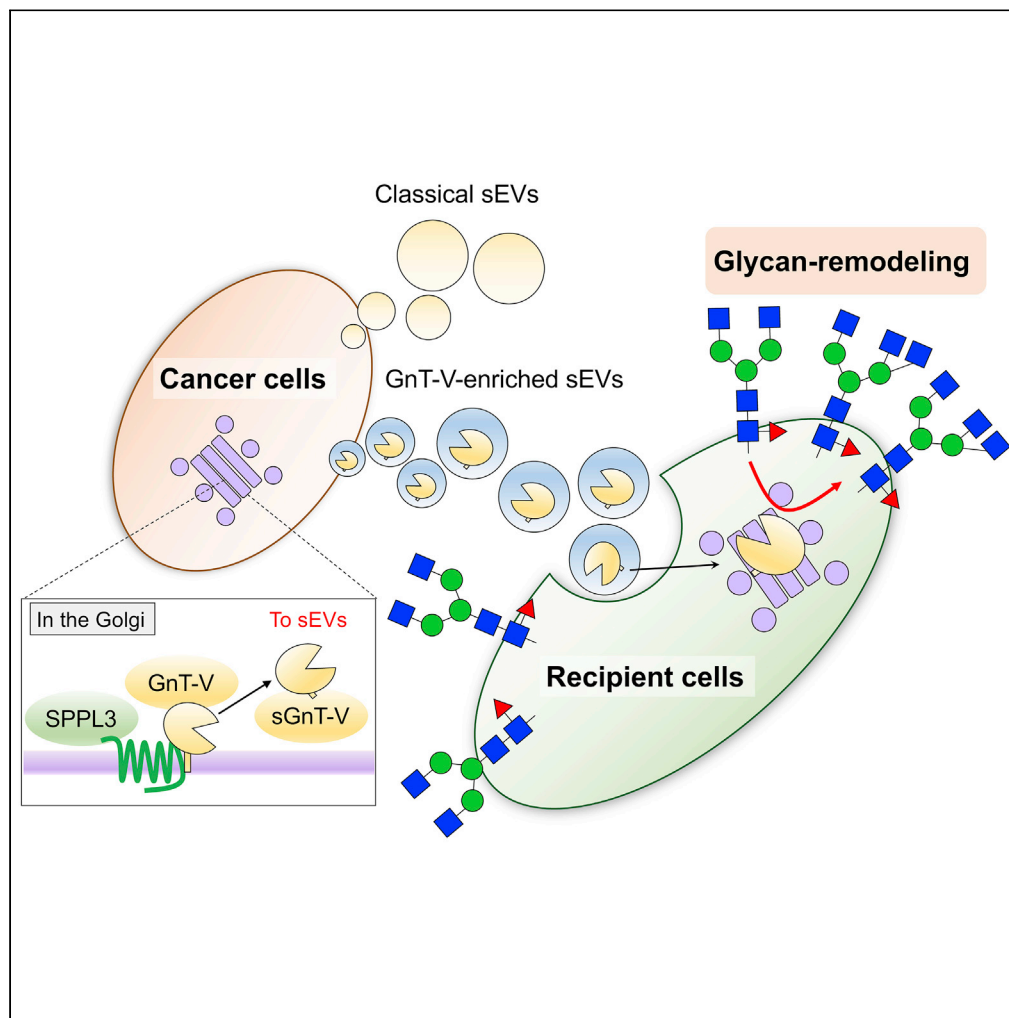## Article

N-acetylglucosaminyltransferase-V (GnT-V)-enriched small extracellular vesicles mediate *N*-glycan remodeling in recipient cells

Tetsuya Hirata, Yoichiro Harada, Koichiro M. Hirosawa, Yuko Tokoro, Kenichi G.N. Suzuki, Yasuhiko Kizuka

kizuka@gifu-u.ac.jp

Highlights

A cancer-related glycosyltransferase, GnT-V, is specifically enriched in sEVs

Cleavage of GnT-V by SPPL3 is important for its enrichment into sEVs

GnT-V-enriched sEVs are distinct from classical exosomes with CD9, CD63, and CD81

GnT-V in sEVs is transferred to recipient cells, remodeling their *N*-glycans

Article

N-acetylglucosaminyltransferase-V (GnT-V)-enriched small extracellular vesicles mediate *N*-glycan remodeling in recipient cells

Tetsuya Hirata,[1] Yoichiro Harada,[2] Koichiro M. Hirosawa,[3] Yuko Tokoro,[1] Kenichi G.N. Suzuki,[3] and Yasuhiko Kizuka[1,4,*]

SUMMARY

Small extracellular vesicles (sEVs) secreted from cancer cells play pivotal roles in cancer metastasis and malignancy by transferring biomolecules and conditioning future metastatic sites. Studies have elucidated structures and functions of glycans on sEVs; however, whether sEVs remodel glycans in recipient cells remains poorly understood. Here, we examined the enzyme activity of glycosyltransferases for complex *N*-glycan biosynthesis in cancer-derived sEVs and discovered that cancer-related glycosyltransferase, *N*-acetylglucosaminyltransferase-V (GnT-V, a.k.a. MGAT5), is selectively enriched in sEVs among various glycosyltransferases. GnT-V in sEVs is a cleaved form, and cleavage by SPPL3 protease is necessary for loading GnT-V in sEVs. Fractionation experiments and single-particle imaging further revealed that GnT-V was enriched in non-exosomal sEVs. Strikingly, we found that enzymatically active GnT-V in sEVs was transferred to recipient cells and the *N*-glycan structures of recipient cells were remodeled to express GnT-V-produced glycans. Our results suggest GnT-V-enriched sEVs' role in glycan remodeling in cancer metastasis.

INTRODUCTION

Cells secrete various types of small extracellular vesicles (sEVs), which contain an abundance of specific cargo molecules, including proteins, miRNA, DNA, lipids, and glycans.[1–3] These cargo-containing sEVs are incorporated by recipient cells and act as tools for cell–cell communication under both physiological and pathological conditions, thereby regulating various cellular functions.[4,5] Increasing evidence suggests that sEVs derived from cancer cells play various significant roles in cancer malignancy, such as promoting proliferation,[6,7] angiogenesis,[8,9] epithelial-to-mesenchymal transition,[10] and organ-specific cancer metastasis by conditioning the pre-metastatic niches.[11–13] However, the molecular mechanisms by which cargo molecules in sEVs regulate cancer malignancy remain unclear.

EVs are categorized by their size.[4] Ectosomes are vesicles generated by the outward budding of the plasma membrane and can be categorized as microvesicles, microparticles, and large vesicles of up to 1,000 nm in diameter. By contrast, exosomes originate from endosomal membranes and range in size from 50 to 200 nm in diameter. The generation of exosomes was reported to be controlled by endosomal protein trafficking and by the formation of intraluminal vesicles (ILVs). For instance, Rab GTPase proteins contribute to exosomal formation by controlling endosomal trafficking.[14,15] In addition, endosomal sorting complexes required for transport (ESCRT),[2,16,17] a lipid ceramide,[18,19] and tetraspanins[20] are required for the generation of ILVs. Recent studies have identified the novel subtypes of sEVs called exomeres and supermeres, which are nanoparticles smaller than classical exosomes (<50 nm in diameter) lacking a membranous vesicular structure.[21,22]

Previous proteomic analyses suggested that the components of exosomes are highly variable among cell types and subtypes.[21,23,24] However, reassessment of the composition of sEVs by high-resolution density gradient fractionation suggested that *bona fide* cargo molecules of exosomes are not as diverse as previously thought and that they mainly contain tetraspanins (CD9, CD63, and CD81) and ESCRT proteins such as Alix and TSG101, but not miRNA or DNA.[25] Consequently, proteins previously considered as components of exosomes, such as RNA binding proteins, miRNA biogenesis proteins, and Rab GTPase proteins,

[1]Laboratory of Glycobiochemistry, Institute for Glyco-core Research (iGCORE), Gifu University, Gifu 501-1193, Japan

[2]Department of Glyco-Oncology and Medical Biochemistry, Osaka International Cancer Institute, Osaka 541-8567, Japan

[3]Laboratory of Cell Biophysics, Institute for Glyco-core Research (iGCORE), Gifu University, Gifu 501-1193, Japan

[4]Lead contact

*Correspondence:
kizuka@gifu-u.ac.jp
https://doi.org/10.1016/j.isci.2022.105747

have been reported to be included in non-exosomal vesicles, in which CD9, CD63, and CD81 are absent, and non-vesicular particles.[25] Similarly, we have categorized sEVs derived from the B16 melanoma cell line by sucrose density gradient flotation assay and found that low-density vesicles were highly enriched with exosomal marker proteins such as CD81 and Alix, whereas high-density fractions largely contained non-exosomal proteins, including Met and tyrosinase.[26] In contrast, other proteins such as metabolism-related proteins, amyloid precursor proteins (APP), β-site APP-cleaving enzyme, and HSP90 were reported to be enriched in exomeres.[21,27] These findings show that sEVs have various types and subtypes with different compositions. To fully understand the biological roles of sEVs, it is pivotal to clarify in more detail the molecular composition of each sEV subset.

Glycoconjugates are also contained in sEVs. Previous studies using a panel of lectins and mass spectrometry showed that the glycan profiles in sEVs differ from those in cells and exhibit a huge variety, depending on the cellular origin.[21,28] Similar to cell surface glycans, sEV glycans have been reported to play various biological roles. For instance, studies have demonstrated that the uptake of sEVs by recipient cells is dependent on N- and O-glycans on sEVs both *in vitro* and *in vivo*.[29,30] Another study revealed that sEVs with higher levels of bisecting N-acetylglucosamine (GlcNAc) branch in N-glycans inhibited the migration of recipient cells by impairing integrin-mediated signals.[31] Glycans in donor cells also regulate the formation of sEVs. Oligomerization of Syndecan mediated by heparan sulfate is required for exosome biogenesis through the Syndecan–Syntenin–Alix axis.[32] In addition, we recently found that blocking of the N-glycosylation pathway in cells strongly inhibits the formation of non-exosomal vesicles mainly containing Met, but not CD81-containing exosomes.[33] Therefore, the importance of glycans for biogenesis and functions of sEVs is being elucidated. However, little is known about how glycosylation of recipient cells is regulated by the uptake of sEVs.

Glycosylation, mediated by concerted actions of many glycosyltransferases, dynamically changes upon the development or aggravation of diseases such as cancer.[34] For instance, β1,6-GlcNAc branch of N-glycan produced by N-acetylglucosaminyltransferase-V (GnT-V, also known as MGAT5) is highly upregulated in various cancer cells,[35] which promotes cancer growth and metastasis by regulating cell adhesion[36] and EGFR signaling.[37] Conversely, *Mgat5*-deficient mice showed greatly reduced tumor growth and metastasis.[38] Therefore, alterations in N-glycan profiles in primary and metastatic cancer cells significantly impact malignancy and could be drug targets. However, because glycosyltransferase-mediated glycosylation is influenced by multiple factors (e.g., enzyme level, acceptor protein trafficking, and sugar metabolism),[39–42] the mechanisms by which N-glycan structures are altered in cancer are not fully understood. In particular, the roles of sEVs in the regulation of glycosylation in recipient cells have barely been studied.

In this study, we set out to explore this issue. We first investigated glycosyltransferase activity in sEVs derived from cancer cell lines and found that GnT-V was specifically enriched. Furthermore, GnT-V-enriched sEVs exerted glycan-modifying activity in recipient cells. Our results indicate the potential contribution of glycan remodeling to cancer metastasis.

RESULTS

An N-glycan branching enzyme, GnT-V, is enriched in sEVs

To obtain sEVs, culture media were first centrifuged to remove cell debris and large extracellular vesicles, including apoptotic bodies and microvesicles. The resultant supernatants were then ultracentrifuged at 100,000 × g for 1 h to precipitate sEVs. Using this method, we isolated sEVs from three cancer cell lines—B16 mouse melanoma, A549 human lung cancer, and Neuro2A (N2A) mouse neuroblastoma—and confirmed that exosome markers (CD63, CD81, and Alix) were highly enriched in the sEV fractions, with the exception of CD63 in the A549 samples (Figure 1A). Nano-pulse analysis using qNano particle analyzer further showed that the average diameters of the particles in the sEV fraction derived from the three cell lines were similar (approximately 100 nm), ranging from 60 to 200 nm (Figure 1B), which is consistent with the typical size of sEVs.

We examined whether the activity of N-glycan branching enzymes was detectable in the sEV fraction. N-Glycosylation is initiated in the ER and is further modified in the Golgi by combined reactions of glycosyltransferases.[44,45] In the Golgi, after the reaction of GnT-II[46] (Figure 1C), N-glycans are branched by the actions of other glycosyltransferases, including GnT-III,[47] GnT-IVa,b,[48,49] GnT-V[50] and FUT8[51,52] (Figure 1C). To examine the
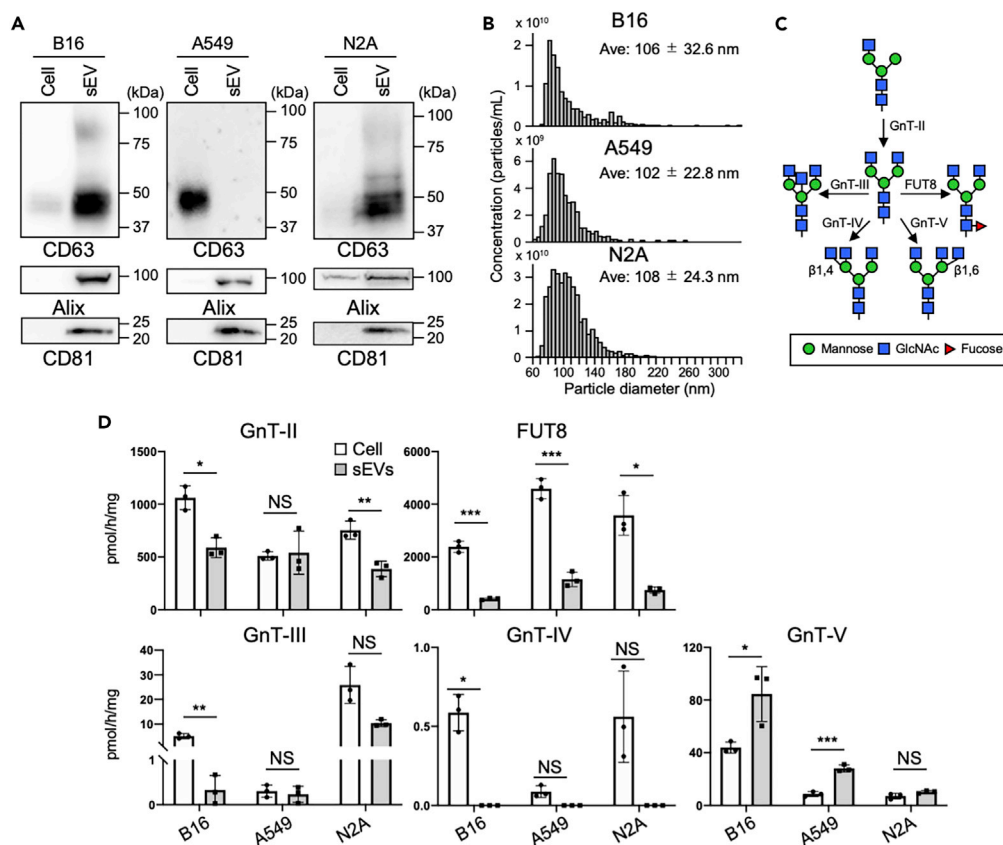
Figure 1. Activity of *N*-glycan biosynthetic enzymes in sEVs isolated from three cancer cell lines

(A) The expression of exosomal marker proteins in cells and sEVs isolated from B16, A549, and N2A cells. CD63, Alix, and CD81 were blotted as exosome markers.

(B) The number and size of sEVs from B16, A549, and N2A cells were measured using qNano. Average particle diameters (Ave) are shown.

(C) Schematic of *N*-glycan branching pathway. The enzymes investigated here are depicted. Glycan symbols are in accordance with symbol nomenclature for glycans.[43]

(D) *In vitro* activities of *N*-glycan branching enzymes in cells and sEVs isolated from B16, A549, and N2A cells were measured using reverse-phase HPLC and specific substrates. For GnT-II activity, GnMbi-PA was used as an acceptor substrate. For GnT-III,-IV, and-V activities, GnGnbi-PA was used as an acceptor substrate. For FUT8 activity, GnGnbi-Asn-PNS was used as an acceptor substrate. Data are represented as mean ± SD (n = 3, number of experiments). Statistical analysis was performed by unpaired Student's *t*test or Mann-Whitney U test. *p< 0.05; **p< 0.005; ***p< 0.0005; NS, not significant. See also Figure S1.

activity of these glycosyltransferases in sEVs, the lysates of sEVs or sEV-producing cells were incubated with acceptor substrates of these enzymes, GnMbi-PA (for GnT-II), GnGnbi-PA (for GnT-III,-IV, and-V), or GnGnbi-Asn-PNS (for FUT8) (Figure S1A), followed by separation of the products from the unreacted substrates by reverse-phase HPLC, as established previously.[53] The elution positions of the enzyme products were confirmed by control reactions using purified recombinant enzymes (Figure S1B). In the cells, we detected the endogenous activity of all enzymes examined (Figures S1C and S1D). Surprisingly, in the sEV fraction from all three cell lines, we also detected the activity of these enzymes, with the exception of GnT-IV (Figures 1D and S1C). In particular, the activity of GnT-V was remarkably higher in sEVs than that in cells (Figure 1D). These results suggest that glycosyltransferases for *N*-glycan branching were included in sEVs as active forms and that GnT-V was selectively enriched into sEVs.

GnT-V in sEVs is a soluble form cleaved by SPPL3

We next performed western blotting of sEVs with anti-GnT-V antibody that can detect endogenous GnT-V (Figure S2). Intriguingly, we found that the electromobility of GnT-V in sEVs derived from B16 and A549 cells was consistently and slightly faster than that in cells (Figure 2A, first and second lanes). This suggests that
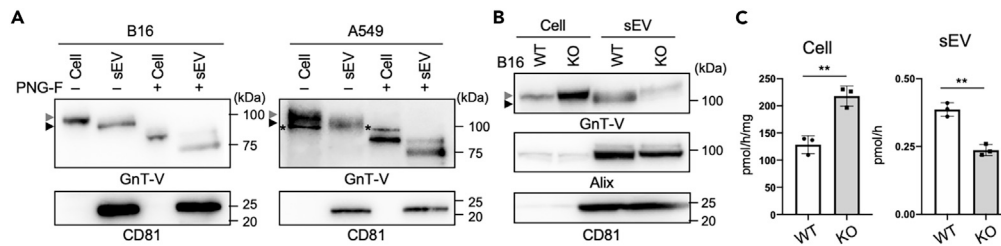
Figure 2. GnT-V enriched in the sEVs is the soluble form cleaved by SPPL3

(A) The cell and sEV lysates of B16 and A549 cells were treated with or without PNGase F (PNG-F). The proteins in the cell and sEV lysates were blotted for GnT-V and CD81. Gray arrowhead indicates full-length GnT-V, black arrowhead indicates sGnT-V cleaved by SPPL3, and asterisks indicate non-specific bands.

(B) The proteins in the cell and sEV lysates of B16 (WT) and B16-SPPL3-KO (KO) cells were treated with or without PNG-F. The proteins in the cell and sEV lysates were blotted for GnT-V, Alix, and CD81. Gray arrowhead indicates full-length GnT-V and black arrowhead indicates sGnT-V cleaved by SPPL3.

(C) The activity of GnT-V in the cell and sEV lysates of B16 (WT) and B16-SPPL3-KO (KO) cells. Data are represented as mean ± SD (n = 3, number of experiments). Statistical analysis was performed by unpaired Student's *t*test. **p< 0.005. See also Figures S2 and S3.

GnT-V in sEVs was modified or cleaved differently from GnT-V in cells. As GnT-V has six *N*-glycosylation sites, we first examined whether the difference in electromobility was because of the structural differences of *N*-glycans. However, even after the removal of all *N*-glycans with peptide *N*-glycanase F (PNG-F), the difference in mobility was still observed (Figure 2A, third and fourth lanes), ruling out the possibility that the difference in mobility was derived from *N*-glycans on GnT-V. Instead, as GnT-V is proteolytically cleaved by SPPL3,[39] we hypothesized that GnT-V in sEVs is a cleaved short form (hereafter designated as "sGnT-V") produced by SPPL3. To examine this, we knocked out SPPL3 in B16 cells[54] and investigated the protein level and activity of GnT-V in sEVs derived from SPPL3-KO cells. The protein level and activity of GnT-V were increased in KO cells (Figure 2B, first and second lanes, and Figure 2C, left). Meanwhile, the sGnT-V protein level and activity were decreased and full-length GnT-V was observed in sEVs derived from SPPL3-KO cells (Figure 2B, third and fourth lanes, and Figure 2C, right). Taking these findings together, we concluded that the enrichment of GnT-V in sEVs is enhanced by the cleavage of GnT-V by SPPL3.

Because free sGnT-V (membrane unbound form of sGnT-V) is also present in the culture media, we wondered if free sGnT-V could bind to sEVs in the culture media. However, only limited fraction of free GnT-V present in the culture media was precipitated together with sEVs prepared from GnT-V-KO B16 cells (Figure S3), implying that most of sGnT-V is loaded onto the sEVs inside the cells.

sGnT-V is mainly present outside of sEVs as oligomers

GnT-V is a type II membrane protein and is cleaved by SPPL3 within the transmembrane domain near the luminal side,[55] producing a luminal soluble form. The presence of soluble sGnT-V in sEVs was unexpected because sEVs, including exosomes, are typically generated by the invagination of endosomal membranes and contain membranous or cytoplasmic molecules, but not soluble luminal ones.[4] On the basis of these findings, there were two possibilities for the presence of sGnT-V in sEVs: sGnT-V could be located outside of sEV being associated with membranes or loaded inside sEVs through an uncharacterized pathway.

To explore these possibilities, we examined the location of GnT-V in sEVs by single-particle imaging and biochemical analyses. The strategy of single-particle imaging is depicted in Figure 3A. C-Terminally Halo-tagged sGnT-V outside of sEVs was first labeled with a membrane-impermeable Halo ligand conjugated with Alexa488 (Halo-Alexa488). sEVs were next incubated with another membrane-permeable Halo ligand conjugated with TMR (Halo-TMR) to stain inner sGnT-V. This allowed us to discriminate sGnT-V outside and inside sEVs using differences in fluorescence (Figure 3A). To first validate our assay system, we expressed CD81 with Halo-tag at the C-terminus (CD81-Halo) or internal position (Halo in-CD81) in which the Halo-tag faces inside or outside of sEVs, respectively (Figure S4A). B16 cells stably expressing CD81-Halo and Halo in-CD81 were established (Figure S4B), and western blotting showed that both CD81-Halo and Halo in-CD81 were present in sEVs (Figure S4C), even though Halo in-CD81 was less efficiently loaded into sEVs. Single-particle imaging of sEVs expressing CD81-Halo and Halo-in CD81 revealed that 97.4%
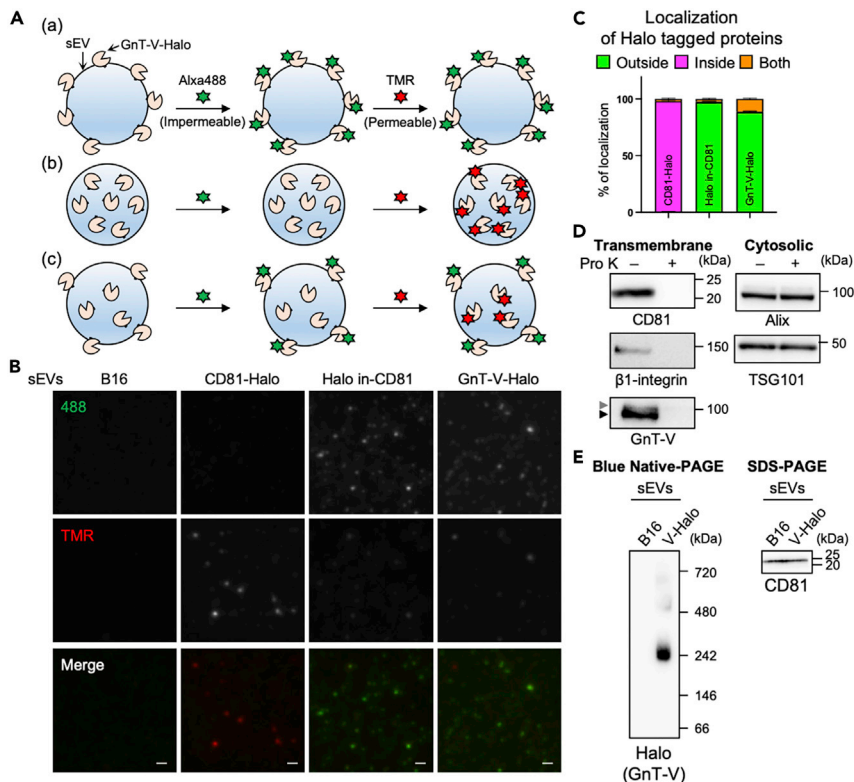
Figure 3. Topology of GnT-V in the sEVs

(A) Schematic of the imaging strategy. (a) If GnT-V-Halo was mostly localized outside of the sEVs, almost all sEVs were stained with membrane-impermeable Halo-tag ligand conjugated with Alexa488 and hardly stained with membrane-permeable Halo-tag ligand conjugated with TMR. (b) If GnT-V-Halo was mostly localized inside of the sEVs, sEVs were hardly stained with Halo-tag ligand conjugated with Alexa488 and instead stained with Halo-tag ligand conjugated with TMR. (c) If GnT-V-Halo was localized both outside and inside sEVs, sEVs were stained with both Halo-tag ligands conjugated with Alexa488 and TMR.

(B) Single-particle imaging of sEVs isolated from B16, CD81-Halo-expressing B16 cells, Halo in-CD81-expressing B16 cells, and GnT-V-Halo-expressing B16 cells. Fluorescence-labeled sEVs were seeded on glass-bottomed dishes and images were acquired. Green, Alexa488 signals; red, TMR signals. Bars: 1 μm.

(C) Topological analysis of CD81-Halo, Halo in-CD81, and GnT-V-Halo in sEVs. Proportions of localization of Halo-tagged proteins outside, inside, or both outside and inside sEVs were calculated from B. Data are represented as mean ± SEM (n = 11 for CD81-Halo and Halo in-CD81 and n = 9 for GnT-V-Halo, number of pictures).

(D) The sEV lysates were treated with or without proteinase K (Pro K) and the proteins were blotted for CD81, β1-integrin, Alix, TSG101, and GnT-V. Gray arrowhead indicates full-length GnT-V and black arrowhead indicates sGnT-V cleaved by SPPL3.

(E) The sEVs lysates were subjected to Blue Native-PAGE (left) or SDS-PAGE (right), and blotted for GnT-V-Halo or CD81. See also Figures S4–S6.

of the particles expressing CD81-Halo were only stained with Halo-TMR, while 97.2% of the particles expressing Halo in-CD81 were only stained with Halo-Alexa488 (Figures 3B and 3C), confirming that our assay system discriminates between inside and outside of sEVs. To next investigate the location of sGnT-V, we generated B16 cells stably expressing GnT-V-Halo (Figure S5A). Western blotting of sEVs revealed that GnT-V-Halo was detected in sEVs (Figure S5B). Surprisingly, single-particle imaging revealed that 0.5% of the particles were only stained with Halo-TMR, and 99.5% of sEVs were Alexa488-positive, indicating that most of the sGnT-V was located outside of sEVs (Figures 3B and 3C).

To verify this finding, we performed a protease protection assay. Isolated sEVs were treated with or without proteinase K (Pro K) under membrane-impermeable conditions, followed by western blotting. We confirmed that transmembrane proteins CD81 and β1-integrin were both Pro K-sensitive and that soluble Alix and TSG101 located inside of sEVs were Pro K-resistant (Figure 3D, left and right panels). Subsequently, we found that GnT-V in sEVs became undetectable after Pro K treatment (Figure 3D, left panel).
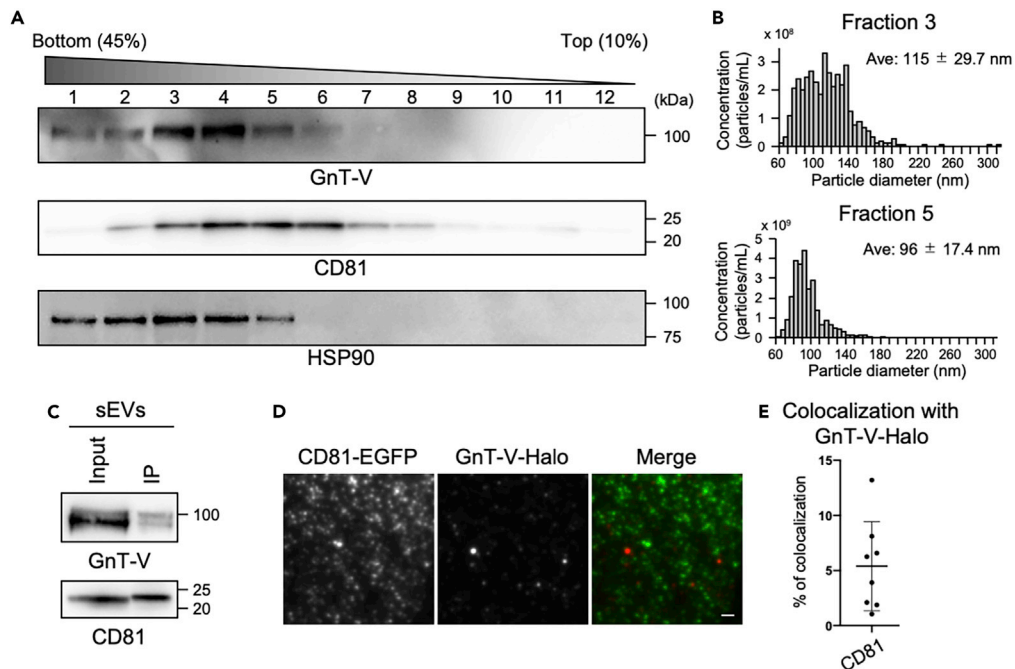
Figure 4. Characterization of GnT-V-enriched sEVs

(A) Sucrose density gradient ultracentrifugation of sEVs from B16. Twelve fractions were blotted for GnT-V, CD81 (marker for exosomes), and HSP90 (marker for exomeres).

(B) The number and size of sEVs in Fractions 3 and 5 in A were measured using qNano. Average particle diameters (Ave) are shown.

(C) Isolation of CD9, CD63, and CD81-positive exosomes from sEVs derived from B16 WT. sEVs lysates (input) and immunoprecipitated samples (IP) were blotted for GnT-V and CD81.

(D) Single-particle imaging of sEVs expressing GnT-V-Halo and CD81-EGFP. Fluorescence-labeled sEVs were seeded on glass-bottomed dishes and images were acquired. Green, CD81-EGFP; red, GnT-V-Halo. Bar: 1 μm.

(E) A graph showing the percentages of colocalization between GnT-V-Halo and CD81-EGFP. Data are represented as mean ± SD (n = 8, number of pictures). See also FigureS7.

We also confirmed that GnT-V in the sEV fraction was solubilized with neutral detergent, similar to exosomal markers, CD81 and CD9 (Figure S6). Because protein aggregates were not solubilized with neutral detergent,[56] this suggests that GnT-V detected in the sEV fraction is associated with membrane but not protein aggregates. These lines of evidence demonstrated that most of sGnT-V is present on the outside of sEVs.

One possible mechanism for the presence of soluble sGnT-V on the outside of sEVs is that sGnT-V interacts with full-length membrane-spanning GnT-V. Because SPPL3 cleaves GnT-V within the transmembrane region,[55] sGnT-V likely contains a stem region that is required for the oligomerization of GnT-V,[57] thereby possibly forming homo-oligomers. To explore this possibility, we took advantage of Blue Native-PAGE. We prepared sEVs from WT B16 or Halo-GnT-V-expressing B16 cells, and the sEV lysates were subjected to Blue Native-PAGE separation, followed by detection with anti-Halo antibody. GnT-V-Halo was detected mainly at around 240 kDa, which corresponds to the size of dimer comprising sGnT-V-Halo (~120 kDa) and GnT-V-Halo (~130 kDa), suggesting that sGnT-V could form homo-oligomers in sEVs (Figure 3E).

GnT-V-enriched sEVs are distinct from exosomes

We next investigated whether sGnT-V is loaded in exosomes or other sEVs. To discriminate the subtypes of sEVs, we carried out fractionation by sucrose density gradient centrifugation. The sEV fraction derived from B16 cells was loaded on the top of the sucrose gradient, followed by ultracentrifugation at 100,000 × g for 18 h. Western blotting of each fraction showed that CD81, an exosome marker, was mainly detected from fractions 3 to 6, whereas HSP90, which is enriched in exomeres, was mainly detected from fractions 1 to 5 (Figure 4A), indicating that different types of sEV were separated by this fractionation. We found that GnT-V

was mainly detected from fractions 1 to 5, which was distinct from the pattern of CD81, suggesting that GnT-V is in non-exosomal sEVs. We also measured the size of sEVs in fraction 3 (mainly containing GnT-V-enriched sEVs) and fraction 5 (mainly containing exosomes), and found that the average particle diameter in fraction 3 was larger (115 ± 29.7 nm) than that in fraction 5 (96 ± 17.4 nm) (Figure 4B). To further examine whether GnT-V is loaded in non-exosomal vesicles, we immunopurified exosomes from isolated sEVs using pan-exosome isolation beads (mixture of anti-CD9, CD63, and CD81 antibody-conjugated beads) and examined whether GnT-V is enriched in the exosomes or not. Western blotting showed that GnT-V was not enriched in the immunopurified exosomes (Figure 4C), indicating that GnT-V is mainly loaded onto non-exosomal sEVs. Furthermore, single-particle imaging of sEVs derived from cells expressing both GnT-V-Halo and EGFP-tagged CD81 (Figures S7A and S7B) showed that only 5% of GnT-V-Halo was colocalized with the exosome marker CD81 (Figures 4D and 4E). Taken together, these results indicated that GnT-V is in non-exosomal sEVs.

Remodeling of N-glycan structures in recipient cells by sEVs

As sGnT-V in sEVs is enzymatically active (Figure 1), we finally explored the possibility that GnT-V-enriched sEVs remodel N-glycans in recipient cells after their incorporation. To this end, GnT-V-negative recipient cells [previously established HeLa-GnT-V-KO cells[58]] were incubated with sEVs derived from B16 cells with or without the expression of GnT-V-Halo. The staining with PHA-L4 lectin, which mainly detects GnT-V producing β1,6-GlcNAc branch of N-glycans,[59] was robustly decreased in HeLa-GnT-V-KO cells as shown previously (Figure S8).[58]

To visualize the internalization of sEVs, we first labeled total sEVs with carboxyfluorescein succinimidyl ester (CFSE) and GnT-V-containing sEVs with Halo-TMR. GnT-V-KO recipient cells were incubated with serum-free medium containing fluorescence-labeled sEVs for 48 h, and cells internalizing sEVs were detected by flowcytometry. We found high levels of CFSE signals in cells treated with sEVs derived from both B16 and B16/GnT-V-Halo (Figure 5A). Furthermore, TMR signals were only detected in cells treated with sEVs expressing GnT-V-Halo, indicating that HeLa-GnT-V-KO cells engulfed GnT-V-enriched sEVs. Next, to examine the N-glycan remodeling of recipient cells, sEV-treated cells were stained with PHA-L4 lectin. The results showed that both TMR and PHA-L4 signals were only detected in cells treated with sEVs expressing GnT-V-Halo (Figure 5B, dot plot and histogram). Similarly, blotting with PHA-L4 lectin was slightly increased in cells treated with sEVs derived from B16 WT cells, but not from B16-GnT-V-KO cells (Figure S9), indicating that sGnT-V-enriched sEVs can remodel N-glycan structures in recipient cells.

The N-glycan alteration in recipient cells could be caused by glycosylation in the recipient cells by transferred GnT-V, direct transfer of already glycosylated proteins, or transfer of Mgat5 mRNA, encoding GnT-V protein. As the expression levels of β1,6-GlcNAc branch in sEVs from B16 and B16/GnT-V-Halo were similar (Figure 5C), these results imply that transferred GnT-V could work as an active enzyme to remodel glycans in recipient cells. To verify whether internalized sGnT-V on sEVs was still active in recipient cells, we measured in vitro enzyme activity in recipient cells treated with sEVs. After 48 h of incubation with sEVs, GnT-V activity was observed in cells treated with sEVs from GnT-V-Halo-expressing cells (Figure 5D, brown line), whereas GnT-V activity was below the limit of detection in cells treated with sEVs from B16 cells (Figure 5D, blue line). This demonstrates that sGnT-V in sEVs is active even after internalization into recipient cells. Finally, we investigated where internalized sGnT-V was located in recipient cells. After cells had been treated with TMR-labeled sEVs for 48 h, they were co-stained with TMR and a Golgi marker, Golgin97. Punctate TMR signals were observed throughout the cells treated with sEVs expressing GnT-V-Halo (Figure 5E), and TMR signals were partially colocalized with those of the Golgi marker (Figure 5E, lower). These results suggest that sGnT-V from sEVs is incorporated into recipient cells as an active form, some of which is transported back to the Golgi.

DISCUSSION

In this study, we explored the impact of the uptake of sEVs on glycan profiles in recipient cells. Our major findings are that sGnT-V produced by SPPL3 is selectively enriched in non-exosomal sEVs, and N-glycan structures in recipient cells are remodeled by GnT-V-enriched sEVs. Although the presence of glycosyltransferases such as GnT-V in the extracellular space, including body fluids and culture media, is well known,[60,61] the glycosyltransferases known to be present in sEVs were limited to ST6Gal1.[27] To our knowledge, the present work has demonstrated for the first time that GnT-V is present on sEVs as an active form. Although cell–cell communication by exosomes is well established, alteration of cellular conditions in recipient cells via non-exosomal sEVs has yet to be well clarified. Our findings provide evidence that
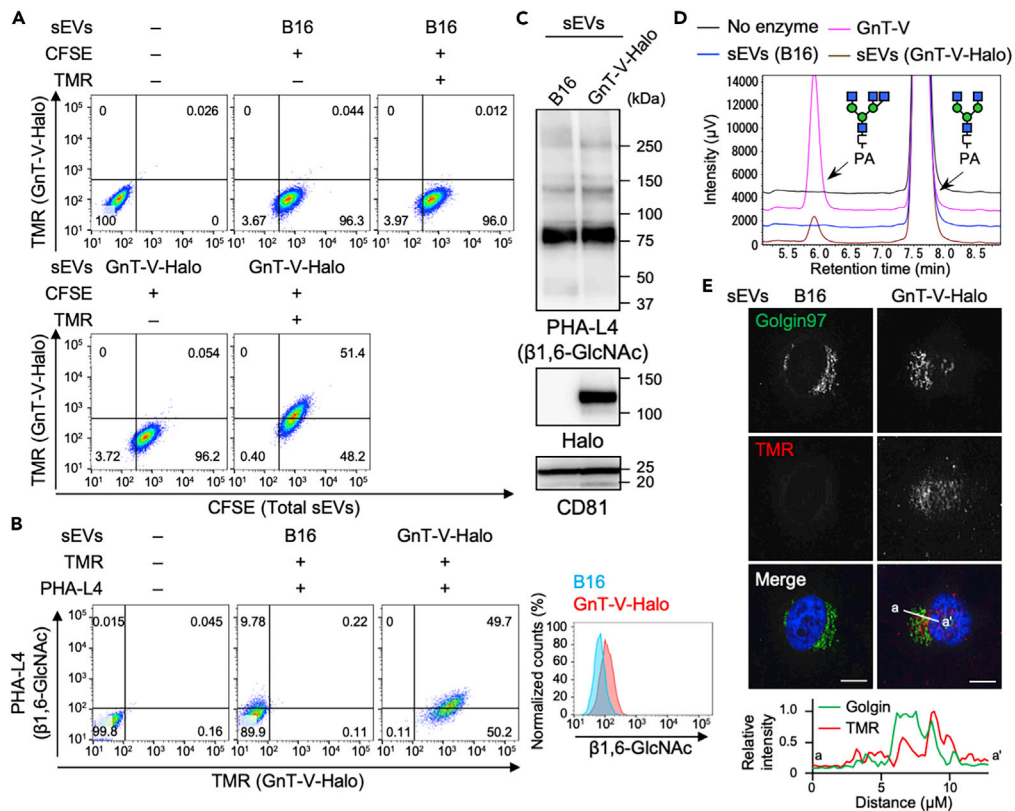
Figure 5. Remodeling of *N*-glycan structures of recipient cells by sEVs

(A) Uptake of sEVs derived from B16 cells into HeLa-GnT-V-KO cells. sEVs labeled with or without fluorescent probes (CFSE and TMR) were added to the culture medium, and cells were further cultured for 48 h. The fluorescence intensities of CFSE (horizontal) and TMR (vertical) were measured and plotted. The numbers in panels indicate the percentage of cells in each region.

(B) Surface expression of β1,6-GlcNAc branch in HeLa-GnT-V-KO cells treated with sEVs derived from B16 or GnT-V-Halo-expressing B16 cells. sEVs labeled with or without TMR were added to the culture medium, and cells were cultured for 48 h. Cells were stained with PHA-L4 conjugated with FITC and fluorescence intensities of TMR (horizontal) and PHA-L4 (vertical) were measured and plotted. The right panel shows histograms of the fluorescence intensities of PHA-L4 in cells treated with sEVs derived from B16 cells or B16 expressing GnT-V-Halo cells.

(C) Proteins from lysates of sEVs derived from B16 and B16 expressing GnT-V-Halo cells were blotted for Halo, CD81, and PHA-L4 lectin.

(D) *In vitro* activity of GnT-V was measured in HeLa-GnT-V-KO cell lysates treated with or without sEVs derived from B16 (blue line) or B16 expressing GnT-V-Halo cells (brown line). Black and pink lines show the negative and positive control experiments without and with recombinant GnT-V, respectively. GnGnbi-PA was used as an acceptor substrate.

(E) (Upper) HeLa-GnT-V-KO cells were treated with or without TMR-labeled sEVs derived from B16 and B16 expressing GnT-V-Halo cells and cultured for 48 h. Intracellular localization of sEVs was examined. (Lower) Line plots indicate the fluorescence intensities relative to the highest signals set as 1. Bars: 10 μm. See also Figures S8 and S9.

non-exosomal sEVs have the ability to modulate glycans in recipient cells. This suggests that not only exosomes but also other sEVs contribute to cancer metastasis and that non-exosomal sEVs are also possible drug targets and biomarkers for cancer treatment.

We investigated five glycosyltransferase activities related to *N*-glycan branching in sEVs and strikingly found that GnT-V was selectively enriched in sEVs. Similar results were observed in three different cancer cell lines (Figure 1D), suggesting that enrichment of GnT-V in sEVs is a common feature in cancer cells. Furthermore, we here revealed that proteolytic cleavage of GnT-V enhances the selective targeting of GnT-V into sEVs (Figure 2). Similarly, not only full-length ST6Gal1, a glycosyltransferase acting on *N*-glycan terminals,[62] but also its cleaved form has been shown to be packaged into sEVs.[27] These findings raise the possibility that proteolytic cleavage of glycosyltransferases could be a trigger for efficient targeting into

sEVs. It will be intriguing to examine whether there are also other glycosyltransferases in sEVs and whether they are present as cleaved forms there. Another possible mechanism for the selective loading into sEVs is that lectin-like proteins preferentially bind to specific *N*-glycan structures to package their cargo into sEVs. Recently, we found that the blockade of *N*-glycan biosynthesis inhibited selective cargo sorting into non-exosomal sEVs.[33] Moreover, we reported that multi-antennary *N*-glycans are highly enriched in sEVs from B16 cells.[63] Because *N*-glycosylation is a fundamental post-translational protein modification in the secretory pathway and has various structures, cells likely use *N*-glycans as markers for selective cargo sorting into sEVs. Investigation of how specific glycosyltransferases are enriched in non-exosomal sEVs could deepen our understanding of the biogenesis and functions of non-exosomal sEVs.

Surprisingly, single-particle imaging revealed that GnT-V in sEVs is a cleaved form and mainly located outside of sEVs as homo-oligomers. Because sGnT-V lack its transmembrane domain, it is reasonable to form homo-oligomers with full-length form of GnT-V outside of sEVs. Another possible explanation to be located on sEVs is the presence of a protein that acts as a cargo receptor for sGnT-V on sEVs. To address these possibilities, analysis of the proteins that interact with sGnT-V in sEVs will be important.

We here showed that treatment with GnT-V-containing sEVs remodeled *N*-glycan profiles in recipient cells. Internalized sGnT-V was still active and detected in puncta throughout the recipient cells and partly observed in the Golgi (Figure 5E). Although we did not identify these puncta, because sEVs could be internalized by phagocytosis or endocytosis,[64] we speculated that they represent endosomes or lysosomes. Therefore, majority of sGnT-V taken up into the recipient cells might be degraded. Because nucleotide sugars, which are donor substrates for glycosyltransferases, are limited in organelles other than the Golgi or ER,[44,65] sGnT-V in recipient cells could function in the Golgi. Because sGnT-V could make homo-oligomers with the membrane-spanning form of GnT-V in sEVs (Figure 3E), uptaken sGnT-V could be stably localized in the Golgi. Alternatively, as enzymatic reactions generally occur rapidly, sGnT-V might be transiently localized in the Golgi and act as an enzyme in the Golgi and/or the other endosomal compartments during trafficking. The relatively weak *N*-glycan remodeling activity compared with the *in vitro* activity in recipient cells may be due to the limited localization of sGnT-V in the Golgi in recipient cells.

In summary, we here reported that cancer-related glycosyltransferase GnT-V is selectively enriched in non-exosomal sEVs, and that uptake of sGnT-V-enriched sEVs modulates *N*-glycan structures in the recipient cells. Given that the levels of GnT-V products are correlated with cancer metastasis and poor prognosis,[66] tumor cells may generate pre-metastatic conditions through the remodeling of *N*-glycan structures by GnT-V in future metastatic sites. Future *in vivo* studies will be required to test this hypothesis and to develop new glycan-targeted therapeutics and biomarkers for cancer.

Limitations of the study

There are several limitations in this study. First, we did not clarify the molecular mechanisms of how sGnT-V is enriched in non-exosomal sEVs. Although proteolytic cleavage by SPPL3 is important for the enrichment into sEVs, how sGnT-V is destined to be loaded into sEVs remains unknown. As discussed in this manuscript, identification of potential sGnT-V receptors such as lectins or other transmembrane proteins would be an attractive future work. Second, it remains elusive whether the glycan remodeling via sEVs could contribute to the cancer metastasis. Although *N*-glycan remodeling in recipient cells was able to be examined by FACS and lectin blotting with PHA-L4 lectin in our hands, the change was only minor, implying that it is insufficient to manipulate cancer malignancy with our protocol. Therefore, it is necessary to incorporate more abundant sEVs to induce more drastic *N*-glycan remodeling in recipient cells. Examination of cell proliferation and migration under those conditions is required to uncover the biological significance of sEVs-mediated *N*-glycan remodeling. Finally, our present work is limited to *in vitro* and *in cellulo* systems. It is necessary to investigate whether the *N*-glycan remodeling by incorporation of sGnT-V-enriched sEVs into recipient cells alters cancer malignancy *in vivo* for the future clinical application of the work.

STAR★METHODS

Detailed methods are provided in the online version of this paper and include the following:

- KEY RESOURCES TABLE
- RESOURCE AVAILABILITY
  - Lead contact

SUPPLEMENTAL INFORMATION

Supplemental information can be found online at https://doi.org/10.1016/j.isci.2022.105747.

ACKNOWLEDGMENTS

AUTHOR CONTRIBUTIONS

Y.K. and Y.H. established the concept of this study. Y.H. performed initial experiments. T.H. and Y.T. performed biochemical experiments and analyzed the data. K.H. and K.G.S. performed single-particle imaging and analyzed the data. K.G.S. and Y.K. supervised this study. T.H. drafted the manuscript, and Y.K. and T.H. revised the manuscript. All authors commented on the manuscript and approved its submission.

DECLARATION OF INTERESTS

The authors declare no competing interests.

REFERENCES

1. van Niel, G., D'Angelo, G., and Raposo, G. (2018). Shedding light on the cell biology of extracellular vesicles. Nat. Rev. Mol. Cell Biol. *19*, 213–228. https://doi.org/10.1038/nrm.2017.125.

2. Mathieu, M., Martin-Jaular, L., Lavieu, G., and Théry, C. (2019). Specificities of secretion and uptake of exosomes and other extracellular vesicles for cell-to-cell communication. Nat.

Cell Biol. *21*, 9–17. https://doi.org/10.1038/s41556-018-0250-9.

3. Tkach, M., and Théry, C. (2016). Communication by extracellular vesicles: where we are and where we need to go. Cell *164*, 1226–1232. https://doi.org/10.1016/j.cell.2016.01.043.

4. Kalluri, R., and LeBleu, V.S. (2020). The biology, function, and biomedical applications of

exosomes. Science *367*, eaau6977. https://doi.org/10.1126/science.aau6977.

5. Wortzel, I., Dror, S., Kenific, C.M., and Lyden, D. (2019). Exosome-mediated metastasis: communication from a distance. Dev. Cell *49*, 347–360. https://doi.org/10.1016/j.devcel.2019.04.011.

6. Hong, B.S., Cho, J.H., Kim, H., Choi, E.J., Rho, S., Kim, J., Kim, J.H., Choi, D.S., Kim, Y.K.,

Hwang, D., and Gho, Y.S. (2009). Colorectal cancer cell-derived microvesicles are enriched in cell cycle-related mRNAs that promote proliferation of endothelial cells. BMC Genom. *10*, 556. https://doi.org/10.1186/1471-2164-10-556.

7. Qu, J.L., Qu, X.J., Zhao, M.F., Teng, Y.E., Zhang, Y., Hou, K.Z., Jiang, Y.H., Yang, X.H., and Liu, Y.P. (2009). Gastric cancer exosomes promote tumour cell proliferation through PI3K/Akt and MAPK/ERK activation. Dig. Liver Dis. *41*, 875–880. https://doi.org/10.1016/j.dld.2009.04.006.

8. Zhou, W., Fong, M.Y., Min, Y., Somlo, G., Liu, L., Palomares, M.R., Yu, Y., Chow, A., O'Connor, S.T.F., Chin, A.R., et al. (2014). Cancer-secreted miR-105 destroys vascular endothelial barriers to promote metastasis. Cancer Cell *25*, 501–515. https://doi.org/10.1016/j.ccr.2014.03.007.

9. Treps, L., Perret, R., Edmond, S., Ricard, D., and Gavard, J. (2017). Glioblastoma stem-like cells secrete the pro-angiogenic VEGF-A factor in extracellular vesicles. J. Extracell. Vesicles *6*, 1359479. https://doi.org/10.1080/20013078.2017.1359479.

10. Le, M.T.N., Hamar, P., Guo, C., Basar, E., Perdigão-Henriques, R., Balaj, L., and Lieberman, J. (2014). miR-200-containing extracellular vesicles promote breast cancer cell metastasis. J. Clin. Invest. *124*, 5109–5128. https://doi.org/10.1172/JCI75695.

11. Hoshino, A., Costa-Silva, B., Shen, T.L., Rodrigues, G., Hashimoto, A., Tesic Mark, M., Molina, H., Kohsaka, S., Di Giannatale, A., Ceder, S., et al. (2015). Tumour exosome integrins determine organotropic metastasis. Nature *527*, 329–335. https://doi.org/10.1038/nature15756.

12. Zhang, H., Deng, T., Liu, R., Bai, M., Zhou, L., Wang, X., Li, S., Wang, X., Yang, H., Li, J., et al. (2017). Exosome-delivered EGFR regulates liver microenvironment to promote gastric cancer liver metastasis. Nat. Commun. *8*, 15016. https://doi.org/10.1038/ncomms15016.

13. Rodrigues, G., Hoshino, A., Kenific, C.M., Matei, I.R., Steiner, L., Freitas, D., Kim, H.S., Oxley, P.R., Scandariato, I., Casanova-Salas, I., et al. (2019). Tumour exosomal CEMIP protein promotes cancer cell colonization in brain metastasis. Nat. Cell Biol. *21*, 1403–1412. https://doi.org/10.1038/s41556-019-0404-4.

14. Ostrowski, M., Carmo, N.B., Krumeich, S., Fanget, I., Raposo, G., Savina, A., Moita, C.F., Schauer, K., Hume, A.N., Freitas, R.P., et al. (2010). Rab27a and Rab27b control different steps of the exosome secretion pathway. Nat. Cell Biol. *12*, 19–30. https://doi.org/10.1038/ncb2000.

15. Hsu, C., Morohashi, Y., Yoshimura, S.I., Manrique-Hoyos, N., Jung, S., Lauterbach, M.A., Bakhti, M., Grønborg, M., Möbius, W., Rhee, J., et al. (2010). Regulation of exosome secretion by Rab35 and its GTPase-activating proteins TBC1D10A-C. J. Cell Biol. *189*, 223–232. https://doi.org/10.1083/jcb.200911018.

16. Choudhuri, K., Llodrá, J., Roth, E.W., Tsai, J., Gordo, S., Wucherpfennig, K.W., Kam, L.C., Stokes, D.L., and Dustin, M.L. (2014). Polarized release of T-cell-receptor-enriched microvesicles at the immunological synapse. Nature *507*, 118–123. https://doi.org/10.1038/nature12951.

17. Nabhan, J.F., Hu, R., Oh, R.S., Cohen, S.N., and Lu, Q. (2012). Formation and release of arrestin domain-containing protein 1-mediated microvesicles (ARMMs) at plasma membrane by recruitment of TSG101 protein. Proc. Natl. Acad. Sci. USA *109*, 4146–4151. https://doi.org/10.1073/pnas.1200448109.

18. Trajkovic, K., Hsu, C., Chiantia, S., Rajendran, L., Wenzel, D., Wieland, F., Schwille, P., Brügger, B., and Simons, M. (2008). Ceramide triggers budding of exosome vesicles into multivesicular endosomes. Science *319*, 1244–1247. https://doi.org/10.1126/science.1153124.

19. Bianco, F., Perrotta, C., Novellino, L., Francolini, M., Riganti, L., Menna, E., Saglietti, L., Schuchman, E.H., Furlan, R., Clementi, E., et al. (2009). Acid sphingomyelinase activity triggers microparticle release from glial cells. EMBO J. *28*, 1043–1054. https://doi.org/10.1038/emboj.2009.45.

20. van Niel, G., Charrin, S., Simoes, S., Romao, M., Rochin, L., Saftig, P., Marks, M.S., Rubinstein, E., and Raposo, G. (2011). The tetraspanin CD63 regulates ESCRT-independent and -dependent endosomal sorting during melanogenesis. Dev. Cell *21*, 708–721. https://doi.org/10.1016/j.devcel.2011.08.019.

21. Zhang, H., Freitas, D., Kim, H.S., Fabijanic, K., Li, Z., Chen, H., Mark, M.T., Molina, H., Martin, A.B., Bojmar, L., et al. (2018). Identification of distinct nanoparticles and subsets of extracellular vesicles by asymmetric flow field-flow fractionation. Nat. Cell Biol. *20*, 332–343. https://doi.org/10.1038/s41556-018-0040-4.

22. Zhang, Q., Jeppesen, D.K., Higginbotham, J.N., Graves-Deal, R., Trinh, V.Q., Ramirez, M.A., Sohn, Y., Neininger, A.C., Taneja, N., McKinley, E.T., et al. (2021). Supermeres are functional extracellular nanoparticles replete with disease biomarkers and therapeutic targets. Nat. Cell Biol. *23*, 1240–1254. https://doi.org/10.1038/s41556-021-00805-8.

23. Kowal, J., Arras, G., Colombo, M., Jouve, M., Morath, J.P., Primdal-Bengtson, B., Dingli, F., Loew, D., Tkach, M., and Théry, C. (2016). Proteomic comparison defines novel markers to characterize heterogeneous populations of extracellular vesicle subtypes. Proc. Natl. Acad. Sci. USA *113*, E968–E977. https://doi.org/10.1073/pnas.1521230113.

24. Choi, D., Montermini, L., Kim, D.K., Meehan, B., Roth, F.P., and Rak, J. (2018). The impact of oncogenic EGFRvIII on the proteome of extracellular vesicles released from glioblastoma cells. Mol. Cell. Proteomics *17*, 1948–1964. https://doi.org/10.1074/mcp.RA118.000644.

25. Jeppesen, D.K., Fenix, A.M., Franklin, J.L., Higginbotham, J.N., Zhang, Q., Zimmerman, L.J., Liebler, D.C., Ping, J., Liu, Q., Evans, R., et al. (2019). Reassessment of exosome composition. Cell *177*, 428–445.e18. https://doi.org/10.1016/j.cell.2019.02.029.

26. Harada, Y., Suzuki, T., Fukushige, T., Kizuka, Y., Yagi, H., Yamamoto, M., Kondo, K., Inoue, H., Kato, K., Taniguchi, N., et al. (2019). Generation of the heterogeneity of extracellular vesicles by membrane organization and sorting machineries. Biochim.Biophys.Acta. Gen. Subj. *1863*, 681–691. https://doi.org/10.1016/j.bbagen.2019.01.015.

27. Zhang, Q., Higginbotham, J.N., Jeppesen, D.K., Yang, Y.P., Li, W., McKinley, E.T., Graves-Deal, R., Ping, J., Britain, C.M., Dorsett, K.A., et al. (2019). Transfer of functional cargo in exomeres. Cell Rep. *27*, 940–954.e6. https://doi.org/10.1016/j.celrep.2019.01.009.

28. Shimoda, A., Sawada, S.I., Sasaki, Y., and Akiyoshi, K. (2019). Exosome surface glycans reflect osteogenic differentiation of mesenchymal stem cells: profiling by an evanescent field fluorescence-assisted lectin array system. Sci. Rep. *9*, 11497. https://doi.org/10.1038/s41598-019-47760-x.

29. Nishida-Aoki, N., Tominaga, N., Kosaka, N., and Ochiya, T. (2020). Altered biodistribution of deglycosylated extracellular vesicles through enhanced cellular uptake. J. Extracell. Vesicles *9*, 1713527. https://doi.org/10.1080/20013078.2020.1713527.

30. Shimoda, A., Tahara, Y., Sawada, S.I., Sasaki, Y., and Akiyoshi, K. (2017). Glycan profiling analysis using evanescent-field fluorescence-assisted lectin array: importance of sugar recognition for cellular uptake of exosomes from mesenchymal stem cells. Biochem.Biophys. Res. Commun. *491*, 701–707. https://doi.org/10.1016/j.bbrc.2017.07.126.

31. Tan, Z., Cao, L., Wu, Y., Wang, B., Song, Z., Yang, J., Cheng, L., Yang, X., Zhou, X., Dai, Z., et al. (2020). Bisecting GlcNAc modification diminishes the pro-metastatic functions of small extracellular vesicles from breast cancer cells. J. Extracell. Vesicles *10*, e12005. https://doi.org/10.1002/jev2.12005.

32. Baietti, M.F., Zhang, Z., Mortier, E., Melchior, A., Degeest, G., Geeraerts, A., Ivarsson, Y., Depoortere, F., Coomans, C., Vermeiren, E., et al. (2012). Syndecan-syntenin-ALIX regulates the biogenesis of exosomes. Nat. Cell Biol. *14*, 677–685. https://doi.org/10.1038/ncb2502.

33. Harada, Y., Nakajima, K., Suzuki, T., Fukushige, T., Kondo, K., Seino, J., Ohkawa, Y., Suzuki, T., Inoue, H., Kanekura, T., et al. (2020). Glycometabolic regulation of the biogenesis of small extracellular vesicles. Cell Rep. *33*, 108261. https://doi.org/10.1016/j.celrep.2020.108261.

34. Mereiter, S., Balmaña, M., Campos, D., Gomes, J., and Reis, C.A. (2019). Glycosylation in the era of cancer-targeted therapy: where are we heading? Cancer Cell

36, 6–16. https://doi.org/10.1016/j.ccell.2019. 06.006.

35. Kang, R., Saito, H., Ihara, Y., Miyoshi, E., Koyama, N., Sheng, Y., and Taniguchi, N. (1996). Transcriptional regulation of the N-acetylglucosaminyltransferase V gene in human bile duct carcinoma cells (HuCC-T1) is mediated by Ets-1. J. Biol. Chem. *271*, 26706– 26712. https://doi.org/10.1074/jbc.271.43. 26706.

36. Guo, H.B., Johnson, H., Randolph, M., and Pierce, M. (2009). Regulation of homotypic cell-cell adhesion by branched N-glycosylation of N-cadherin extracellular EC2 and EC3 domains. J. Biol. Chem. *284*, 34986–34997. https://doi.org/10.1074/jbc. M109.060806.

37. Partridge, E.A., Le Roy, C., Di Guglielmo, G.M., Pawling, J., Cheung, P., Granovsky, M., Nabi, I.R., Wrana, J.L., and Dennis, J.W. (2004). Regulation of cytokine receptors by Golgi N-glycan processing and endocytosis. Science *306*, 120–124. https://doi.org/10. 1126/science.1102109.

38. Granovsky, M., Fata, J., Pawling, J., Muller, W.J., Khokha, R., and Dennis, J.W. (2000). Suppression of tumor growth and metastasis in Mgat5-deficient mice. Nat. Med. *6*, 306–312. https://doi.org/10.1038/73163.

39. Voss, M., Künzel, U., Higel, F., Kuhn, P.H., Colombo, A., Fukumori, A., Haug-Kröper, M., Klier, B., Grammer, G., Seidl, A., et al. (2014). Shedding of glycan-modifying enzymes by signal peptide peptidase-like 3 (SPPL3) regulates cellular N-glycosylation. EMBO J. *33*, 2890–2905. https://doi.org/10.15252/ embj.201488375.

40. Kizuka, Y., and Taniguchi, N. (2016). Enzymes for N-glycan branching and their genetic and nongenetic regulation in cancer. Biomolecules *6*, 25. https://doi.org/10.3390/ biom6020025.

41. Xiang, Y., Zhang, X., Nix, D.B., Katoh, T., Aoki, K., Tiemeyer, M., and Wang, Y. (2013). Regulation of protein glycosylation and sorting by the Golgi matrix proteins GRASP55/65. Nat. Commun. *4*, 1659. https:// doi.org/10.1038/ncomms2669.

42. Lau, K.S., Partridge, E.A., Grigorian, A., Silvescu, C.I., Reinhold, V.N., Demetriou, M., and Dennis, J.W. (2007). Complex N-glycan number and degree of branching cooperate to regulate cell proliferation and differentiation. Cell *129*, 123–134. https://doi. org/10.1016/j.cell.2007.01.049.

43. Varki, A., Cummings, R.D., Aebi, M., Packer, N.H., Seeberger, P.H., Esko, J.D., Stanley, P., Hart, G., Darvill, A., Kinoshita, T., et al. (2015). Symbol nomenclature for graphical representations of glycans. Glycobiology *25*, 1323–1324. https://doi.org/10.1093/glycob/ cwv091.

44. Schjoldager, K.T., Narimatsu, Y., Joshi, H.J., and Clausen, H. (2020). Global view of human protein glycosylation pathways and functions. Nat. Rev. Mol. Cell Biol. *21*, 729–749. https:// doi.org/10.1038/s41580-020-00294-x.

45. Narimatsu, Y., Büll, C., Chen, Y.H., Wandall, H.H., Yang, Z., and Clausen, H. (2021). Genetic glycoengineering in mammalian cells. J. Biol. Chem. *296*, 100448. https://doi. org/10.1016/j.jbc.2021.100448.

46. Tan, J., D'Agostaro, A.F., Bendiak, B., Reck, F., Sarkar, M., Squire, J.A., Leong, P., and Schachter, H. (1995). The human UDP-N-acetylglucosamine: alpha-6-D-mannoside-beta-1, 2- N-acetylglucosaminyltransferase II gene (MGAT2). Cloning of genomic DNA, localization to chromosome 14q21, expression in insect cells and purification of the recombinant protein. Eur. J. Biochem. *231*, 317–328. https://doi.org/10.1111/j.1432-1033.1995.tb20703.x.

47. Nishikawa, A., Ihara, Y., Hatakeyama, M., Kangawa, K., and Taniguchi, N. (1992). Purification, cDNA cloning, and expression of UDP-N-acetylglucosamine: beta-D-mannoside beta-1, 4N-acetylglucosaminyltransferase III from rat kidney. J. Biol. Chem. *267*, 18199–18204.

48. Oguri, S., Minowa, M.T., Ihara, Y., Taniguchi, N., Ikenaga, H., and Takeuchi, M. (1997). Purification and characterization of UDP-N-acetylglucosamine: alpha1, 3-D-mannoside beta1, 4-N-acetylglucosaminyltransferase (N-acetylglucosaminyltransferase-IV) from bovine small intestine. J. Biol. Chem. *272*, 22721–22727. https://doi.org/10.1074/jbc. 272.36.22721.

49. Yoshida, A., Minowa, M.T., Takamatsu, S., Hara, T., Ikenaga, H., and Takeuchi, M. (1998). A novel second isoenzyme of the human UDP-N-acetylglucosamine:alpha1, 3-D-mannoside beta1, 4-N-acetylglucosaminyltransferase family: cDNA cloning, expression, and chromosomal assignment. Glycoconj. J. *15*, 1115–1123. https://doi.org/10.1023/a:1006951519522.

50. Shoreibah, M., Perng, G.S., Adler, B., Weinstein, J., Basu, R., Cupples, R., Wen, D., Browne, J.K., Buckhaults, P., Fregien, N., and Pierce, M. (1993). Isolation, characterization, and expression of a cDNA encoding N-acetylglucosaminyltransferase V. J. Biol. Chem. *268*, 15381–15385.

51. Uozumi, N., Yanagidani, S., Miyoshi, E., Ihara, Y., Sakuma, T., Gao, C.X., Teshima, T., Fujii, S., Shiba, T., and Taniguchi, N. (1996). Purification and cDNA cloning of porcine brain GDP-L-Fuc:N-acetyl-beta-D-glucosaminide alpha1→6fucosyltransferase. J. Biol. Chem. *271*, 27810–27817. https://doi. org/10.1074/jbc.271.44.27810.

52. Yanagidani, S., Uozumi, N., Ihara, Y., Miyoshi, E., Yamaguchi, N., and Taniguchi, N. (1997). Purification and cDNA cloning of GDP-L-Fuc:N-acetyl-beta-D-glucosaminide:alpha1-6 fucosyltransferase (alpha1-6 FucT) from human gastric cancer MKN45 cells. J. Biochem. *121*, 626–632. https://doi.org/10. 1093/oxfordjournals.jbchem.a021631.

53. Takamatsu, S., Korekane, H., Ohtsubo, K., Oguri, S., Park, J.Y., Matsumoto, A., and Taniguchi, N. (2013). N-acetylglucosaminyltransferase (GnT) assays using fluorescent oligosaccharide acceptor substrates: GnT-III, IV, V, and IX (GnT-Vb).

Methods Mol. Biol. *1022*, 283–298. https:// doi.org/10.1007/978-1-62703-465-4_21.

54. Hirata, T., Takata, M., Tokoro, Y., Nakano, M., and Kizuka, Y. (2022). Shedding of N-acetylglucosaminyltransferase-V is regulated by maturity of cellular N-glycan. Commun.Biol. *5*, 743. https://doi.org/10. 1038/s42003-022-03697-y.

55. Kuhn, P.H., Voss, M., Haug-Kröper, M., Schröder, B., Schepers, U., Bräse, S., Haass, C., Lichtenthaler, S.F., and Fluhrer, R. (2015). Secretome analysis identifies novel signal Peptide peptidase-like 3 (Sppl3) substrates and reveals a role of Sppl3 in multiple Golgi glycosylation pathways. Mol. Cell. Proteomics *14*, 1584–1598. https://doi.org/ 10.1074/mcp.M115.048298.

56. Shaw, B.F., Lelie, H.L., Durazo, A., Nersissian, A.M., Xu, G., Chan, P.K., Gralla, E.B., Tiwari, A., Hayward, L.J., Borchelt, D.R., et al. (2008). Detergent-insoluble aggregates associated with amyotrophic lateral sclerosis in transgenic mice contain primarily full-length, unmodified superoxide dismutase-1. J. Biol. Chem. *283*, 8340–8350. https://doi.org/10. 1074/jbc.M707751200.

57. Sasai, K., Ikeda, Y., Tsuda, T., Ihara, H., Korekane, H., Shiota, K., and Taniguchi, N. (2001). The critical role of the stem region as a functional domain responsible for the oligomerization and Golgi localization of N-acetylglucosaminyltransferase V.The involvement of a domain homophilic interaction. J. Biol. Chem. *276*, 759–765. https://doi.org/10.1074/jbc.M004972200.

58. Hirata, T., Nagae, M., Osuka, R.F., Mishra, S.K., Yamada, M., and Kizuka, Y. (2020). Recognition of glycan and protein substrates by N-acetylglucosaminyltransferase-V. Biochim.Biophys.Acta.Gen. Subj. *1864*, 129726. https://doi.org/10.1016/j.bbagen. 2020.129726.

59. Cummings, R.D., and Kornfeld, S. (1982). Characterization of the structural determinants required for the high affinity interaction of asparagine-linked oligosaccharides with immobilized Phaseolus vulgaris leukoagglutinating and erythroagglutinating lectins. J. Biol. Chem. *257*, 11230–11234.

60. Kim, Y.S., Perdomo, J., and Whitehead, J.S. (1972). Glycosyltransferases in human blood.I.Galactosyltransferase in human serum and erythrocyte membranes. J. Clin. Invest. *51*, 2024–2032. https://doi.org/10. 1172/JCI107008.

61. Kim, Y.S., Perdomo, J., Whitehead, J.S., and Curtis, K.J. (1972). Glycosyltransferases in human blood. II. Study of serum galactosyltransferase and N-acetylgalactosaminyltransferase in patients with liver diseases. J. Clin. Invest. *51*, 2033–2039. https://doi.org/10.1172/JCI107009.

62. Hennet, T., Chui, D., Paulson, J.C., and Marth, J.D. (1998). Immune regulation by the ST6Gal sialyltransferase. Proc. Natl. Acad. Sci. USA *95*, 4504–4509. https://doi.org/10.1073/pnas.95. 8.4504.

63. Harada, Y., Kizuka, Y., Tokoro, Y., Kondo, K., Yagi, H., Kato, K., Inoue, H., Taniguchi, N., and Maruyama, I. (2019). N-glycome inheritance from cells to extracellular vesicles in B16 melanomas. FEBS Lett. *593*, 942–951. https://doi.org/10.1002/1873-3468.13377.

64. French, K.C., Antonyak, M.A., and Cerione, R.A. (2017). Extracellular vesicle docking at the cellular port: extracellular vesicle binding and uptake. Semin. Cell Dev. Biol. *67*, 48–55. https://doi.org/10.1016/j.semcdb.2017.01.002.

65. Caffaro, C.E., and Hirschberg, C.B. (2006). Nucleotide sugar transporters of the Golgi apparatus: from basic science to diseases. Acc. Chem. Res. *39*, 805–812. https://doi.org/10.1021/ar0400239.

66. Murata, K., Miyoshi, E., Kameyama, M., Ishikawa, O., Kabuto, T., Sasaki, Y., Hiratsuka, M., Ohigashi, H., Ishiguro, S., Ito, S., et al. (2000). Expression of N-acetylglucosaminyltransferase V in colorectal cancer correlates with metastasis and poor prognosis. Clin. Cancer Res. 6, 1772–1777.

67. Ihara, H., Tsukamoto, H., Taniguchi, N., and Ikeda, Y. (2013). An assay for alpha 1, 6-fucosyltransferase (FUT8) activity based on the HPLC separation of a reaction product with fluorescence detection. Methods Mol. Biol. *1022*, 335–348. https://doi.org/10.1007/978-1-62703-465-4_25.

68. Koyama-Honda, I., Ritchie, K., Fujiwara, T., Iino, R., Murakoshi, H., Kasai, R.S., and Kusumi, A. (2005). Fluorescence imaging for monitoring the colocalization of two single molecules in living cells. Biophys. J. *88*, 2126–2136. https://doi.org/10.1529/biophysj.104.048967.

STAR★METHODS

KEY RESOURCES TABLE

REAGENT or RESOURCE	SOURCE	IDENTIFIER
Antibodies		
Mouse anti-CD63 (clone NVG-2)	Biolegend	Cat#143902; RRID: AB_11204263
Mouse anti-CD81 (clone B11)	Santa Cruz	Cat#sc-166029; RRID: AB_2275892
Mouse anti-Alix (clone 1A12)	Santa Cruz	Cat#sc-53540; RRID: AB_673819
Mouse anti-β1-integrin	BD Biosciences	Cat#610467; RRID: AB_2128060
Rabbit anti-CD9	Abcam	Cat#ab92726; RRID: AB_10561589
Rabbit anti-TSG101	Abcam	Cat#ab125011: RRID: AB_10974262
Rabbit anti-HSP90 (clone C45G5)	Cell Signaling Technology	Cat#4877; RRID: AB_2233307
Rabbit anti-Golgin97 (clone D8P2K)	Cell Signaling Technology	Cat#13192S; RRID: AB_2798144
Mouse anti-GAPDH (clone 6C5)	Millipore	Cat#MAB374; RRID: AB_2107445
Mouse anti-GnT-V (clone 706824)	R&D Systems	Cat#MAB5469; RRID: AB_10972310
HRP-conjugated anti-mouse IgG	GE Healthcare	Cat#NA931V
HRP-conjugated anti-rabbit IgG	GE Healthcare	Cat#NA934V
Alexa 488-conjugated anti-rabbit IgG	ThermoFisher Scientific	Cat#A21206
Bacterial and virus strains		
XL-10 Gold Ultraompetent cells	Agilent Technologies	Cat#200315
Chemicals, peptides, and recombinant proteins		
Halo-tag Alexa 488 ligand	Promega	Cat#G1002
Halo-tag TMR ligand	Promega	Cat#G8251
CFSE	Bay Bioscience	Cat#13-0850-U500
PNGase F	Roche	Cat#11365169001
cOmplete Mini Protease Inhibitor Cocktail	Roche	Cat#11836170001
Lipofectamine 3000	ThermoFisher Scientific	Cat#L3000
Polyethylenimine (PEI) MAX	Polysciences	Cat#24765
NEBuilder HiFi DNA Assembly Master Mix	New England Biolabs	Cat#E2621
Critical commercial assays		
QuickChange Lightning Site-Directed Mutagenesis kit	Agilent Technologies	Cat#210518-5
Pierce BCA Protein Assay Kit	ThermoFisher Scientific	Cat#23227
Peroxidase Labeling Kit–NH_2	DOJINDO	Cat#LK11
Exosome Isolation Kit Pan, mouse	Miltenyi Biotec	Cat#130-117-039
Experimental models: Cell lines		
Neuro-2A	ATCC	CCL-131
B16	RIKEN cell bank	RCB1283
A549	ATCC	CCL-185
B16-SPPL3-KO (clone #1)	Hirata et al.[54]	N/A
HeLa-GnT-V-KO	Hirata et al.[58]	N/A
B16-hGnT-V-Halo7	Hirata et al.[54]	N/A
B16-CD81-Halo	This study	N/A
B16-Halo in-CD81	This study	N/A
B16-hGnT-V-Halo7-CD81-EGFP	This study	N/A

Continued

REAGENT or RESOURCE	SOURCE	IDENTIFIER
Oligonucleotides		
Primers for constructing all of the plasmids, see Table S1	This study	N/A
Recombinant DNA		
pcDNA6/myc-His A-hGnT-V-Halo7	Hirata et al.[54]	N/A
pEGFPN1/CD81-Halo7	This study	N/A
pcDNA6/CD81-EGFP	This study	N/A
pcDNA6/CD63-EGFP	This study	N/A
pcDNA6/Halo in-CD81	This study	N/A
pX330-Puro-mMGAT5#1	This study	N/A
pX330-Puro-mMGAT5#1	This study	N/A
Software and algorithms		
Izon Control Suite 3.3.2.2001	Izon	https://support.izon.com/qnano-control-suite-software
FlowJo 10.7.1	BD Biosciences	https://www.flowjo.com
GraphPad Prism 8 software	GraphPad Software, Inc.	https://www.graphpad.com

RESOURCE AVAILABILITY

Lead contact

Further information and requests for resources and reagents should be directed to and will be fulfilled by the lead contact, Yasuhiko Kizuka (kizuka@gifu-u.ac.jp).

Materials availability

Reagents generated in this study are available from the lead contact with a completed Materials Transfer Agreement.

Data and code availability

This paper does not report original code.

Any additional information required to reanalyze the data reported in this paper is available from the lead contact upon request.

EXPERIMENTAL MODEL AND SUBJECT DETAILS

All cell lines used in this study for cellular assays are listed in the key resources table. B16 cells were obtained from RIKEN Cell bank and A549, and Neuro2A were obtained from the American Type Culture Collection. B16 expressing hGnT-V-Halo7, B16-SPPL3-KO (clone #1), and HeLa-GnT-V-KO (clone #11) cells were established previously.[54,58] Cells were cultured in Dulbecco's modified Eagle's medium (DMEM) supplemented with 10% fetal bovine serum and 50 μg/mL kanamycin at 37°C under 5% v/v CO_2. Stable transfectants expressing GnT-V-Halo and Halo in-CD81 were maintained in DMEM supplemented with 10% fetal bovine serum, 50 μg/mL kanamycin, and 8 μg/mL blasticidin and cells stably expressing CD81-Halo were maintained in DMEM supplemented with 10% fetal bovine serum, 50 μg/mL kanamycin, and 800 μg/mL G418 under the same conditions. Cells stably expressing both GnT-V-Halo and CD81-EGFP were maintained in DMEM supplemented with 10% fetal bovine serum, 50 μg/mL kanamycin, 8 μg/mL blasticidin, and 800 μg/mL G418 under the same conditions.

METHOD DETAILS

Plasmid construction

Primers used in this study were listed in Table S1. pcDNA6-myc-His A/hGnT-V-Halo7 was constructed previously.[54] To construct pEGFP-N1/CD81-Halo7, pEGFP-N1 vector containing Halo7-tag sequence was amplified by PCR using primers (F: ACCGGTGGTGGGCGCGCC and R: GAATTCAGATCCGGTACCGC)

from pEGFP-N1/CD63-Halo7 and CD81 sequence was amplified by PCR using primers (F: gcggtacc ggatctgaattcATGGGAGTGGAGGGCTGC and R: gaggcgcgcccaccaccggtGTACACGGAGCTGTTCCG) from pFN21AE5228 plasmid purchased from Kazusa Genome Technologies (product ID: FHC08124). The amplified sequences were ligated with NEBuilder HiFi DNA Assembly Master Mix, in accordance with the manufacturer's protocol. To construct pcDNA6/CD81-EGFP, pcDNA6/CD63-EGFP was constructed and used as a template for PCR amplification of the sequence of pcDNA6 containing EGFP sequence using primers (F: ACCGGTGGTGGGCGCGCC and R: GAATTCAGATCCGGTACCGC). CD81 sequence was amplified as described above and the amplified sequences were ligated with NEBuilder HiFi DNA Assembly Master Mix. For the construction of pcDNA6/CD63-EGFP plasmid, pcDNA6 sequence and EGFP-tagged CD63 sequence were amplified from pcDNA6-myc-His A using primers (F: GTTTAAACCCGCTGATCAG and R: gaattcagatccggtaccgcAACTAGCCAGCTTGGGTC) and pEGFP-N1/CD63-EGFP using primers (F: ctggctagttgcggtaccggatctgaattcATGGCGGTGGAAGGAGGAATG and R: gctgatcagcgggtttaaacTTACTTGTACAGCTCGTCCATGC), respectively, and the amplified sequences were ligated with NEBuilder HiFi DNA Assembly Master Mix. To construct pcDNA6/Halo in-CD81, pcDNA6/ACP in-CD81-EGFP and pcDNA6/ACP in-CD81 were constructed. The vector sequence of pcDNA6/ACP in-CD81-EGFP was amplified from pcDNA6/CD81-EGFP using primers (F: acatcaacggcc accaggcgAACCTCCTGTATCTGGAGCTG and R: cgttcttcgatagtgctcatGGTGGTCTGCGGGTCATG) and ACP tag sequence was amplified from pEGFP-N1/ACP-ITGB1 using primers (F: ATGAGCACTATCGAA GAACGCG and R: CGCCTGGTGGCCGTTGAT). The amplified sequences were ligated with NEBuilder HiFi DNA Assembly Master Mix. To construct pcDNA6/ACP in-CD81, pcDNA6 sequence containing ACP-tagged CD81 sequences was amplified using primers (F: TAAGTTTAAACCCGCTGATCAGC and R: gatcagcgggtttaaacttaGTACACGGAGCTGTTCCG) and ligated with NEBuilder HiFi DNA Assembly Master Mix. To construct pcDNA6/Halo in-CD81, pcDNA6 vector containing CD81 sequence was amplified by PCR using primers (F: cgacgctcgagatttccggcAACCTCCTGTATCTGGAGCTG and R: ccagtaccgatttctgccatGG TGGTCTGCGGGTCATG) from pcDNA6/ACP in-CD81 and Halo7 sequence was amplified from pFN21AB7332 purchased from Kazusa Genome Technologies (product ID: FHC05544). The amplified sequences were ligated with NEBuilder HiFi DNA Assembly Master Mix. pX330-Puro-mMGAT5#1 and #2 were generated by digesting pX330-Puro plasmid[58] with BbsI followed by ligation with the annealed primer sets: gRNA#1 (F: caccGTACATTAAGGCACTGGCAG and R: aaacCTGCCAGTGCCTTAATGTAC) and gRNA#2 (F: caccGCTGTCATGACACCAGCGTA and R: aaacTACGCTGGTGTCATGACAGC).

Establishment of stable transfectants

To generate cells stably expressing Halo-tagged CD81, pEGFP-CD81-Halo7 and pcDNA6-Halo in-CD81 plasmids were transfected into B16 cells. Two days after transfection, cells were selected with 800 μg/mL G418 and 8 μg/mL blasticidin for CD81-Halo and Halo in-CD81, respectively. After 1 week of culture, transfectants were further selected by sorting those with positivity for Halo-TMR ligand staining. Sorted cells were further selected by cell sorting with Halo-TMR ligand. To generate cells stably expressing both GnT-V-Halo and CD81-EGFP, pcDNA6-CD81-EGFP plasmid was transfected into B16 cells stably expressing GnT-V-Halo. Two days after transfection, cells were selected by sorting those with positivity for EGFP signal. EGFP-positive cells were further selected with 800 μg/mL G418 and enriched by another round of cell sorting.

Generation of B16-GnT-V-KO cell line

To generate the B16-GnT-V-KO cell line, two different pX330-Puro plasmids harboring sgRNAs targeting the *Mgat5* gene were transfected, as described below. One day after transfection, cells were selected with 3 μg/mL puromycin.

Plasmid transfection

Cells at approximately 50% confluence grown in 6-cm dishes were transfected with each plasmid using Lipofectamine 3000 reagent, in accordance with the manufacturer's protocol.

Preparation of sEVs

Cells grown in 15-cm dishes were washed with PBS twice and cultured in DMEM supplemented with 50 μg/mL kanamycin at 37°C under 5% v/v CO_2 for 48 h. Culture media were collected and centrifuged at 1,200 × g for 5 min to remove cell debris. The supernatants were concentrated with Amicon-Ultra filter units (cut-off 10 kDa, Millipore) by centrifugation at 3,900 × g for 30 min at 4°C. The concentrated samples were then centrifuged at 10,000 × g for 30 min at 4°C to remove large sEVs including microvesicles. The

supernatants were then ultracentrifuged in an S55A2 rotor (himac) at 100,000 × g for 60 min at 4°C. The pellets were washed with 30 μL of PBS once, followed by dissolving with PBS or lysis buffer [20 mM Tris (pH7.4), 150 mM NaCl, 1% Triton X-100, protease inhibitor cocktail] by sonication. To discriminate protein aggregates, the lysate in the lysis buffer was further ultracentrifuged in an S55A2 rotor (himac) at 100,000 × g for 60 min at 4°C. The supernatant was collected and the pellet was dissolved with the same volume of 1 × Laemmli SDS sample buffer and incubated at 95°C for 5 min.

For use in uptake experiments, sEVs were stained with both 10 μM CFSE and 50 nM TMR-labeled Halo ligand or TMR-labeled Halo ligand only at 37°C, followed by purification with a MicroBio-Spin 6 Column.

Isolation of pan-exosomes (CD9, CD81, and CD63-positive exosomes) from crude sEVs from B16 cells was achieved with Exosome Isolation Kit Pan mouse (Miltenyi Biotec, Cat#130-117-039) according to manufacturer protocol. Briefly, crude sEVs prepared as described above were incubated with 50 μL of Exosome Isolation Microbeads for 1 h at room temperature. The samples were loaded onto μ Columns equilibrated with Equilibration Buffer in the magnetic field of the μMACS Separator, and the columns were washed with 200 μL of Isolation Buffer four times. After removing the columns from the magnetic separator, pan-exosomes were eluted with 100 μL of Isolation Buffer.

qNano

sEVs were collected as described above and dissolved in 30 μL of PBS. The particle number and size were measured with qNano (Izon), in accordance with the manufacturer's protocol. Data were analyzed using Izon Control Suite 3.3.2.2001 (Izon).

Ten-fold dilution of sEVs in PBS was used for the analysis with the following settings: nanopores of NP150 (lot numbers: A62693 and A62687 for Figures 1B and 4B, respectively) stretching to 47 mm, and pressure of 5 mbar for B16 and N2A in Figure 2B or 7 mbar for A549 in Figure 2B and B16 in Figure 4B, yielding 100–120 nA of measurement current. The samples were calibrated with 100 nm polystyrene calibration beads (CPC100) that were diluted in PBS.

Sample preparation

Cells were washed with PBS twice and collected by cell scrapers, followed by precipitation by centrifugation at 1,400 × g for 3 min. The cell pellets were lysed with lysis buffer [20 mM Tris (pH7.4), 150 mM NaCl, 1% Triton X-100, protease inhibitor cocktail] by sonication. Protein concentration was measured using a BCA kit.

For PNGase F treatment, samples were denatured in denaturing buffer [20 mM Tris (pH7.4), 0.5% SDS, 1% 2ME, 5 mM EDTA] at 95°C for 5 min, followed by five-fold dilution with Tris-buffered saline (TBS) containing Nonidet P-40 (final concentration, 0.5%). Then, 60 μL of the samples was incubated with 3 μL of water or PNGase F at 37°C for more than 2 h. The samples were then mixed with 5 × Laemmli SDS sample buffer and incubated at 95°C for 5 min.

Measurement of glycosyltransferase activities

Activities of GnT-II, GnT-III,-IV,-V, and FUT8 in the cell lysate and sEVs were measured as described below.[53,67] For GnT-II activity, 3 μL of the cell lysates or sEV lysates was incubated in a total of 10 μL of GnT-III reaction buffer [125 mM MES (pH 6.25), 10 mM MnCl$_2$, 200 mM GlcNAc, 0.5% Triton X-100, and 1 mg/mL BSA] supplemented with 20 mM UDP-GlcNAc and 5 μM fluorescence-labeled acceptor N-glycan substrate (GnMbi-PA) at 37°C for 1 h. For GnT-III,-IV, and-V activities, 3 μL of the cell lysates or sEV lysates was incubated in a total of 10 μL of GnT-III reaction buffer supplemented with 20 mM UDP-GlcNAc and 10 μM fluorescence-labeled biantennary acceptor N-glycan substrate [GnGnbi-PA (PA, 2-aminopyridine)] at 37°C for 3 h. For FUT8 activity, 0.5 μL of cell lysates or 3 μL of sEV lysates was incubated in a total of 10 μL of FUT8 reaction buffer [100 mM MES (pH 7.0), 200 mM GlcNAc, 0.5% Triton X-100, and 1 mg/mL BSA] supplemented with 1 mM GDP-fucose and 10 μM fluorescence-labeled biantennary acceptor N-glycan substrate {GnGnbi-Asn-PNS; PNS, N-[2-(2-pyridylamino)ethyl] succinamidyl} at 37°C for 30 min (for cell lysates) or 1 h (for sEV lysates). For GnT-V activity in HeLa-GnT-V-KO cells treated with or without sEVs derived from B16 expressing hGnT-V-Halo7, 3 μL of the cell lysates was incubated in a total of 10 μL of GnT-V reaction buffer [125 mM MES (pH 6.25), 10 mM EDTA, 200 mM GlcNAc, 0.5% Triton X-100, and 1 mg/mL BSA] supplemented with 20 mM

UDP-GlcNAc and 10 μM GnGnbi-PA at 37°C for 16 h. After enzymatic reactions, the samples were boiled at 99°C for 2 min to inactivate the enzymes and 40 μL of water was added. After centrifugation at 21,500 × g for 5 min, the supernatants were analyzed by reverse-phase HPLC with an ODS column (4.6 × 150 mm, TSKgel ODS-80TM; TOSOH Bioscience). HPLC analysis was conducted in the isocratic mode in which 80% buffer A (20 mM ammonium acetic buffer (pH 4.0)) and 20% buffer B (1% butanol in buffer A) were loaded at 1 mL/min.

Single-particle imaging of sEVs

sEVs were collected from B16 cells or B16 cells expressing hGnT-V-Halo, CD81-Halo, Halo in-CD81, or both hGnT-V-Halo and CD81-Halo, grown in 1 × 15-cm dishes, and dissolved in 50 μL of PBS. For topological investigation of hGnT-V-Halo as shown in Figure 3B, sEVs were stained with 1 μM Halo-tag Alexa488 ligand for 30 min at 37°C, followed by staining with 500 nM TMR-labeled Halo ligand for 30 min at 37°C. For the characterization of sGnT-V-enriched sEVs as shown in Figure 4C, sEVs were stained with 50 nM TMR-labeled Halo ligand for 30 min at 37°C. sEVs were purified with a MicroBio-Spin 6 Column and dissolved in 50 μL of PBS. sEVs were seeded on glass-bottomed dishes (35 mm in diameter with a glass window of 12 mm in diameter, 0.15-mm-thick glass; Iwaki) and images were acquired with a custom-built objective lens-type TIRF microscope, based on a Nikon Ti-E equipped with a 100×, 1.49 NA objective lens (400× total magnification). The sEVs on the glass surface were locally illuminated with evanescent fields of 488 nm (EXCSR-488C-100-CDRHG-W; Spectra-Physics) and 561 nm (Jive 300; Cobolt) laser lines (50 μm in diameter). For the dual-color single-particle imaging, the dual-color images were separated by a 560-nm dichroic mirror (T560LPXR; Chroma) for Alexa488/TMR, and were projected into two detection arms with band-pass filters for Alexa488 (ET525/50m; Chroma) and for TMR (ET600; Chroma). The fluorescence signal in each channel was amplified by a two-stage microchannel-plate image intensifier (C9016-02; Hamamatsu Photonics), and the intensified image was projected onto the sCMOS camera (ORCA-Fusion C14440; Hamamatsu Photonics), synchronized with the other camera placed on the other detection arm, operated at 30 Hz. The image sequences in each channel were superimposed after correction for spatial distortions, using a C++-based computer program produced in-house.[68] The image analysis was performed by a series of macros in ImageJ (FIJI) software. First, we averaged the movies for 10 frames (30 fps) to reduce the noise. Second, we binarized the images using "Lee methods." Third, we counted the number of particles using "Analyze Particles." For detection of the co-stained particles, we used a multiplied image of the binarized images of two channels.

Sucrose density gradient ultracentrifugation

sEVs were collected from B16 cells grown in 6 × 15-cm dishes (approximately 1 × 10⁸ cells) and dissolved in 300 μL of PBS. To prepare the sucrose density gradient, 6.5 mL of 10% (w/v) sucrose solution [10 mM Tris-HCl (pH = 7.5)] was loaded into a 13.2 mL ultracentrifugation tube, followed by addition of the same amount of 45% (w/v) sucrose solution [10 mM Tris-HCl (pH = 7.5)] at the bottom of the tube. A 10%–45% (w/v) sucrose gradient was generated by Gradient Master (BioComp Instruments, Inc.) using an optimal protocol. Then, 300 μL of sEV samples were gently loaded on the top of the tube. sEVs were separated by ultracentrifugation in an SW41 Ti rotor (Beckmann Coulter) at 100,000 × g for 18 h at 4°C with no brake. Twelve fractions were collected from the bottom of the tube using a peristaltic pump (ATTO). To concentrate sEVs, collected fractions were diluted with 1.6 mL of PBS and further ultracentrifuged at 200,000 × g for 1 h at 4°C. The pellets were lysed with lysis buffer [20 mM Tris (pH7.4), 150 mM NaCl, 1% Triton X-100, protease inhibitor cocktail] by sonication.

Testing for the binding of free sGnT-V to sEVs in the culture media

For collecting the culture medium containing free sGnT-V, post-sEVs supernatants were prepared from B16 WT or GnT-V-Halo expressing cells grown on two 15-cm dishes as described in *Preparation of sEVs* section, and the small aliquots were taken and mixed with 5 × Laemmli SDS sample buffer for western blotting. sEVs prepared from GnT-V-KO B16 cells grown on one 15-cm dish were mixed with residual post-sEVs supernatants. The mixture was subjected to pipetting 30-40 times, followed by incubation for 30 min at room temperature. The mixture was then ultracentrifuged in an S55A2 rotor (himac) at 100,000 × g for 60 min at 4°C. The supernatants were mixed with 5 × Laemmli SDS sample buffer, and the ppt was suspended in 60 μL of 1 × Laemmli SDS sample buffer, followed by sonication and boiling at 95°C for 5 min.

Western and lectin blotting

The same amounts of proteins were loaded in each well and separated by 5%–20% SDS-PAGE, followed by transfer to nitrocellulose membranes. For western blotting, the membranes were blocked with 5% skim milk in TBS containing 0.1% Tween-20 (TBS-T) for 30 min, followed by incubation with primary antibodies diluted with 5% skim milk/TBS-T overnight at 4°C. After washing with TBS-T three times, the membranes were incubated with secondary antibodies conjugated with HRP for 1 h at room temperature. For lectin blotting with HRP-conjugated lectins, the membranes were blocked with 1% BSA/TBS-T overnight at 4°C, followed by incubation with HRP-conjugated lectins diluted with 1% BSA/TBS-T. Signals were detected using FUSION SOLO 7s EDGE (Vilber). Dilution rates of antibodies and lectins were as follows: anti-CD63 (1:500); anti-CD81 (1:300); anti-Alix (1:1,000); anti-CD9 (1:500); anti-β1-integrin (1:200); anti-TSG101 (1:1,000); anti-HSP90 (1:500); anti-GnT-V (1:300); anti-GAPDH (1:2,000); PHA-L4-HRP (1:2,000); anti-mouse IgG-HRP (1:5,000); and anti-rabbit IgG-HRP (1:15,000).

Blue Native PAGE

Sample preparation for Blue Native PAGE was performed using NativePAGE Sample Prep Kit (Novex) according to the manufacturer's protocol. Briefly, sEVs were suspended on ice in sample buffer (supplied in the kit) containing 1% digitonin and protease inhibitor mixture (Fujifilm). After ultracentrifugation at 100,000 $\times$ g for 30 min at 4°C, the supernatants were collected. A portion of the supernatant was directly analyzed by SDS-PAGE and Western blotting with anti-CD81 antibody. For NativePAGE, NativePAGE G-250 (0.25% at the final concentration) was added to the supernatant, and proteins were separated by 4-16% native PAGE with NativePAGE Running Buffer (Novex) and cathode buffer (Novex) and then transferred to a PVDF membrane. Proteins on the PVDF membrane were fixed with 8% acetic acid, and the membranes were washed with methanol. The methods for blocking, antibody incubation, and signal detection were the same as those described for Western blotting.

FACS analysis

To examine Halo expression in cells, cells stably expressing Halo-tagged proteins were washed with PBS twice and collected by cell scrapers, followed by precipitation by centrifugation at 1,400 $\times$g for 3 min. The cells were stained with 50 nM TMR-labeled Halo ligand in PBS on ice for 25 min, followed by washing with PBS twice. To examine the uptake of sEVs, HeLa-GnT-V-KO cells grown in 12-well dishes were treated with or without sEVs derived from B16 cells stably expressing hGnT-V-Halo7 [grown in 1 $\times$ 15-cm dishes (about 1.5 $\times$ 10^7 cells/dish)] stained with both CFSE and TMR-labeled Halo ligand for 48 h. To monitor N-glycan remodeling in the recipient cells, HeLa-GnT-V-KO cells were grown in 12-well dishes and treated with or without sEVs derived from B16 cells stably expressing hGnT-V-Halo7 for 48 h. The cells were stained with FITC-labeled PHA-L4 lectin (1:200) and TMR-labeled Halo ligand in PBS on ice for 25 min, followed by washing with PBS twice. Data were collected with a FACS Melody cell sorter and analyzed by FlowJo software (BD Biosciences).

Lectin blotting of HeLa-GnT-V-KO cells after treatment with sEVs

sEVs were collected from B16 WT or B16-GnT-V-KO cells grown on 3 $\times$ 15-cm dishes (about 1.5 $\times$ 10^7 cells/dish), and dissolved in PBS. HeLa-GnT-V-KO cells were cultured on 1 $\times$ 3.5-cm dish (about 2 $\times$ 10^6 cells/dish) for the recipient cells, and treated with sEVs dissolved in PBS or PBS as negative control for 48 h. Cells were collected and lysed, and blotting with PHA-L4 lectin was performed as described above.

Immunofluorescence imaging of cells treated with fluorescence-labeled sEVs

HeLa-GnT-V-KO cells were seeded on an eight-well chamber slide and treated with or without sEVs derived from B16 cells stably expressing hGnT-V-Halo7 grown in 1 $\times$ 15-cm dishes (approximately 1.5 $\times$ 10^7 cells). Two days after treatment, cells were washed with PBS twice, followed by fixation with 4% PFA in PBS at room temperature for 15 min. After washing with PBS twice, cells were blocked and permeabilized with blocking buffer (3% BSA, 0.1% Nonidet P-40 in PBS) by incubating at room temperature for 30 min. The cells were then incubated with primary antibodies at room temperature for 1 h. After washing with PBS three times, the cells were incubated with fluorescence probe-conjugated secondary antibodies and DAPI at room temperature for 1 h. After washing with PBS three times, the samples were mounted with Prolong diamond antifade reagent (ThermoFisher Scientific). Fluorescence images were obtained using a BZX-800 (KEYENCE) with sectioning function. Line plot was generated using

ImageJ FIJI software and relative fluorescence intensity was plotted. Dilution rates of antibodies and a Halo ligand were as follows: anti-Golgin97 (1:200), anti-rabbit IgG-Alexa488 (1:2000), and DAPI (1:5000).

QUANTIFICATION AND STATISTICAL ANALYSIS

Statistical analyses and graphing were performed using GraphPad Prism 8 software (GraphPad Software, Inc.).